Title

Optimization and sensitivity of a global biogeochemistry ocean model using combined in situ DIC, alkalinity, and phosphate data

Journal

Journal of Geophysical Research, 113(C8)

ISSN

0148-0227

Authors

Kwon, EY
Primeau, F

Publication Date

2008-08-07

DOI

10.1029/2007JC004520

Low-frequency radar sounding of temperate ice masses in Southern Alaska

E. Rignot,[1,2] J. Mouginot,[1] C. F. Larsen,[3] Y. Gim,[2] and D. Kirchner[4]

Received 24 July 2013; revised 1 October 2013; accepted 2 October 2013; published 16 October 2013.

[1] We present the Warm Ice Sounding Explorer (WISE), a low-frequency (2.5 MHz) radar for the sounding of temperate ice. WISE deployment in southern Alaska in 2008 and 2012 provides comprehensive measurements of glacier thickness, reveals deep valleys beneath glaciers and the full extent of zones grounded below sea level. The east branch of Columbia Glacier is deeper that its main branch and remains below sea level 20 km farther inland. Ice is 1000 m deep on Tazlina Glacier. On Bering glacier, two sills separate three deep bed depressions (>1200 m) that coincide with the dynamic balance lines during surges. The piedmont lobe of Malaspina Glacier and the lower reaches of Hubbard Glacier are entirely grounded below sea level 40 and 10 km, respectively, from their termini. Knowledge of ice thickness in these regions helps better understand their glacier dynamics, mass balance, and impact on sea level. **Citation:** Rignot, E., J. Mouginot, C. F. Larsen, Y. Gim, and D. Kirchner (2013), Low-frequency radar sounding of temperate ice masses in Southern Alaska, *Geophys. Res. Lett.*, *40*, 5399–5405, doi:10.1002/2013GL057452.

1. Introduction

[2] Glaciers in many parts of the world, including Antarctica, are changing rapidly in response to climate change [e.g., *Jacob et al.*, 2012]. Yet for many of them we do not have good measurements for ice thickness and bed topography. Radar sounding is the main tool for such measurements, but this technique is problematic in regions where ice is temperate, i.e., at the melting point throughout the ice column, e.g., in Alaska [*Molnia*, 2008] or Patagonia; or partly temperate, e.g., along coastal sectors of Greenland [*Clarke and Echelmeyer*, 1996] or in subantarctic islands [*Blindow et al.*, 2010]. In the presence of temperate ice, volume clutter from englacial heterogeneities, i.e., liquid-water-filled pockets, cracks, veins, and conduits, occlude radar echoes from the bed when observed at the higher frequencies, typically above 5 MHz [*Smith and Evans*, 1972; *Watts and England*, 1976]. This difficulty often cannot be overcome with more radiative power or radiative elements, but success has been found through the use of longer radar wavelengths. Prior studies indicate that optimal frequencies for reducing volume clutter are between 1 MHz and 5 MHz, i.e., the size of water-filled cavities is smaller than 30 to 160 m in ice. Glaciers with rough, crevassed, and broken surfaces that flow through deep, narrow channels yield excessive surface clutter that provides additional challenge for radar sounders.

[3] Major advances in radar sounding have taken place in the 1990s, e.g., with the development of the Multichannel Coherent Radar Depth Sounder (MCoRDS) at the University of Kansas, and which includes GPS tagging, digital recording, and digital processing [*Gogineni et al.*, 2001]. These radars operate at a high frequency, typically 60–150 MHz, with chirps and multiple antennas to yield higher performance levels, but the frequency limitation still precludes their use on temperate ice. This leaves a void of ice thickness data on temperate ice masses that put a fundamental limit on analyses of ongoing and future glacier changes and impact on sea level.

[4] Surface-based radars operating at 1 to 2.5 MHz have been used to survey temperate ice in Alaska, but bed echoes rarely exceed 800–850 m in depth, and data collection is limited and not well distributed [e.g., *Arcone and Yankielun*, 2000; *Gades et al.*, 2012; *Molnia*, 2008]. Most radar data have been collected on moderate to small-sized glaciers, accessible in the summer months, only in the ablation area, where ice thickness is not maximal. In areas of thicker ice, these systems are limited.

[5] The first airborne radio-echo sounding of a temperate glacier was conducted in 1978 on Columbia Glacier, Alaska [*Brown et al.*, 1986]. The sounding system operated at 1.5 MHz, but did not include a precise recording of the airplane position, used a primitive recording and digitizing system, and had time constraints for development and application. Even though the system worked well to depths of 400 m, the program was discontinued.

[6] In 2006, we developed a new airborne radar system operating at low frequency, high power, to address the challenges of measuring temperate ice thickness and complement existing airborne systems. We deployed the radar system in March 2006 in Alaska along with another airborne system from the University of Washington, Seattle [*Conway et al.*, 2009], but our system did not reach full maturity until year 2008. Here we present the radar design and data collected in Alaska in November 2008 and March 2012. We discuss our observations of ice thickness in these regions and their relevance on glacier dynamics and mass balance.

2. Data and Methodology

2.1. Radar Design

[7] The design of the Warm Ice Sounding Explorer (WISE) radar sounder is based on the Mars Advanced Radar

[1]Department of Earth System Science, University of California, Irvine, California, USA.
[2]Jet Propulsion Laboratory, California Institute of Technology, Pasadena, California, USA.
[3]Geophysical Institute, University of Alaska Fairbanks, Fairbanks, Alaska, USA.
[4]Department of Physics and Astronomy, University of Iowa, Iowa City, Iowa, USA.

Corresponding author: E. Rignot, Department of Earth System Science, University of California, Irvine, CA 92697, USA. (erignot@uci.edu)

0094-8276/13/10.1002/2013GL057452

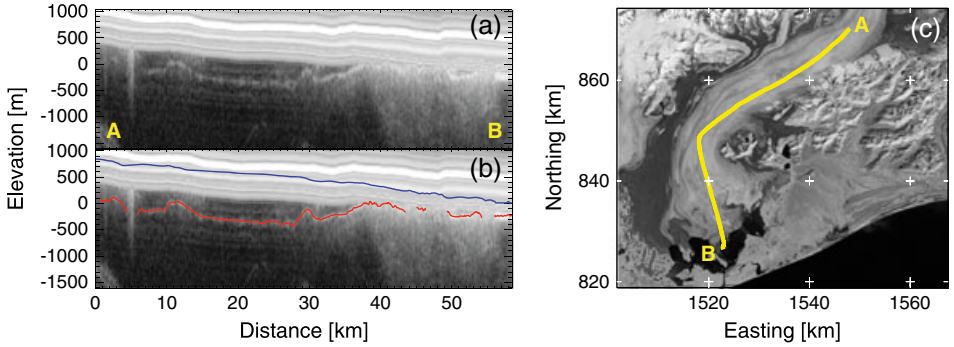

Figure 1. (a) WISE radar echogram acquired at 2.5 MHz in March 2012 over the Bering Glacier, Alaska along profile A-B from the upper part of Bering to its terminus, with vertical scale in meters and horizontal scale in kilometers; (b) interpreted echogram with surface position from laser altimetry (blue) and bed position from WISE (red). Surface return is clipped from the radar data due to the low flying altitude of the aircraft. (c) geographic location of profile A-B overlaid on a MODIS mosaic of the region in an Universal Transverse Mercator (UTM) projection.

for Subsurface and Ionosphere Sounding (MARSIS) radar [*Jordan et al.*, 2009]. The radar system consists of a single transmitter and receiver operating on a dipole antenna deployed in the back of the airplane. The transmitter from the University of Iowa is a high power, limited duty cycle instrument designed to produce high-amplitude radio frequency (RF) tone bursts derived from a continuous wave RF signal or an externally generated RF tone burst. The radar wave generator and timing are synchronized using the same radar clock. The receiver is a conventional receiver from Ritec™. Instead of using a transmit-receive switch, we use a diplexer, so that the receiver is always connected to the antenna, yet it is isolated from the initial high-voltage transmit burst. The data from the receiver comes directly into the analog-digital converter inside a National Instrument™ computer through a 100 Mb/s bus and stored on disk in chunks of 5 min of data. The resistively loaded wire antenna is constructed inside a 120 m long static rope. Electrically, it is damped to minimize ringing, which allows operation at low altitude and a frequency range from 1 to 5 MHz at the expense of a reduced radiated power level of 1–2 W. Due to its length, the antenna is released and retracted in the air via a small opening on the aircraft floor. To lower the antenna below the aircraft belly, a Teflon drogue and counterweight is attached to the end of the antenna to maintain a shallow antenna angle of about 30° in flight. This allows the antenna to extend down and stay away from the aircraft fuselage and tail. The antenna is electrically coupled with the airplane structure. The antenna design is optimized using a model simulation by the University of Iowa to maximize coupling with the transmitter/receiver. The radar design is best suited for planes much smaller in size than the radar wavelength (120 m in air). The total weight of the radar including rack is 50 kg.

[8] The radar is operated at a center frequency of 2.5 MHz, with a sampling frequency of 20 MHz on 16 bits with a 50 μs data window, and a pulse repetition frequency of 1 kHz. The default operating power is 800 W peak power. The radar is fully programmable and controlled using a LabView™ interface. The radar is flown nominally at an altitude of about 1000 m above the glacier surface. Flying at a lower altitude increases spatial resolution and reduces surface clutter but clips radar returns from the surface. Clipping of the surface returns limits the saturation of the radar receiver, which results in a higher signal-to-noise ratio for the bed returns. A conventional GPS receiver is operated at 20 Hz along with the radar, with a precision of 10 m, which is sufficient for our application.

2.2. Processing

[9] The first stage of data processing is an incoherent averaging of radar echoes in the azimuth direction, followed by a range migration using an Omega-K algorithm [*Stolt*, 1978]. The resulting echo diagrams are semiautomatically digitized to record the position of the ice surface and of the glacier bed. In March 2012, WISE operated at 400 m above the surface, hence clipping the surface returns. The surface reference was provided by NASA IceBridge's University of Alaska, Fairbanks (UAF) LiDAR Scanner [*Johnson et al.*, 2013], which was operated simultaneously on a DHC-3 Otter from Ultima Thule Lodge. The LiDAR is based on a Riegl LMS-Q240i scanner. The nominal precision of detection of the bed is 1/4 of the wavelength at 2.5 MHz or 17 m in ice. The LiDAR picks up the surface return within an accuracy of 20 cm, hence yielding a nominal precision in thickness of 17 m.

[10] Where surface elevation is not recorded by the LiDAR, we employ a digital elevation model (DEM) from the Shuttle Radar Mapping Mission and from Intermap Technologies, Inc. (ITI), both acquired in the year 2000 [*Muskett et al.*, 2009], which we adjust vertically at both ends of the missing surface segments and linearly interpolate in between to best fit the UAF laser elevation data of March 2012 and account for ice elevation change between 2000 and 2012. This data filling occurs over less than 30% of the flight tracks.

2.3. Study Sites

[11] We deployed WISE on the Bering, Bagley, Malaspina, Seward, and Hubbard glaciers in November 2008 and also on the Columbia and Tazlina glaciers in March 2012. Surface conditions were cold and dry in March 2012, but warm and wet in October 2008, hence, data quality is lower in 2008.

[12] The Bering Glacier System, which comprises the Bering Glacier, the Bagley Ice Valley (BIV) and smaller tributaries, and ice valleys, is the largest and longest (200 km) glacier in North America. It flows from the

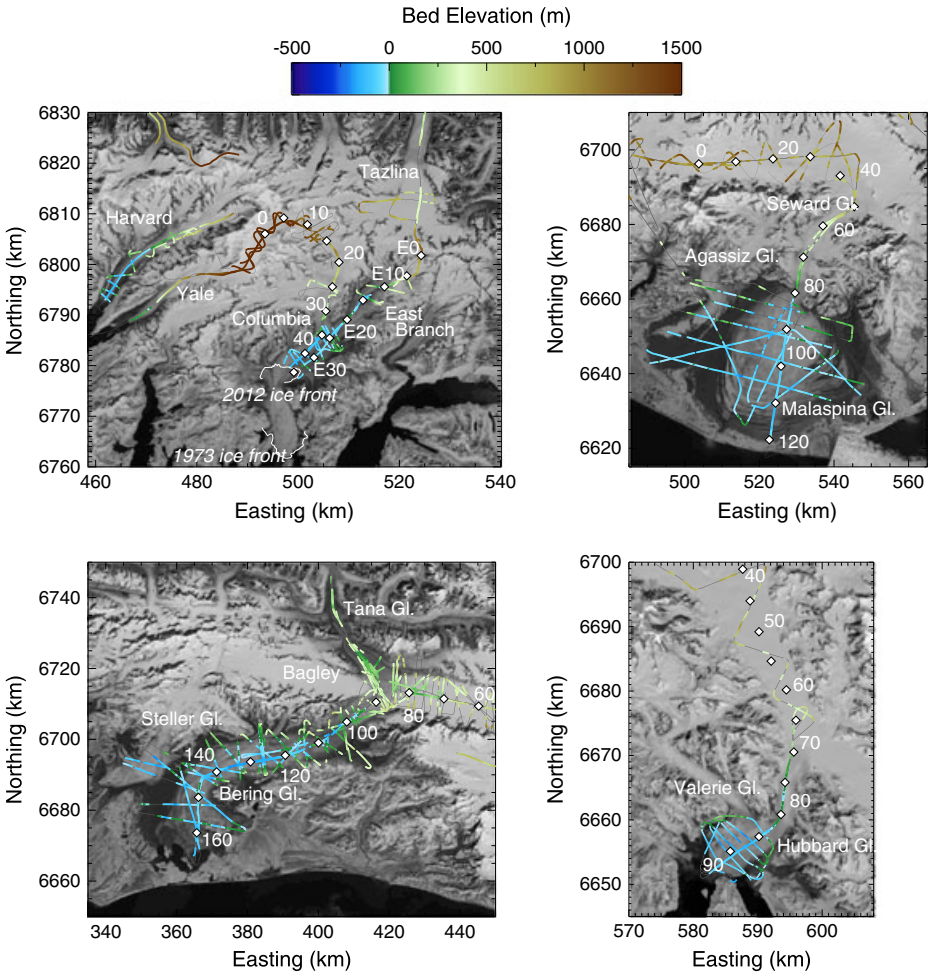

Figure 2. (first panel) Bed elevation and (second panel) ice thickness of four major glacier regions of Southern Alaska mapped with WISE in November 2008 and WISE/UAF LiDAR in March 2012. The color-coded results are overlaid on a MODIS mosaic of the glaciers. For each glacier system, the origin of distance is the glacier head, consistent with historical practices [*Molnia*, 2008]. Distances are marked by a white diamond every 5 or 10 km. Ice front positions in 1973 and 2012 are indicated for Columbia Glacier.

St. Elias Mountains and terminates in Vitus Lake near the Gulf of Alaska. The glacier has thinned several hundred meters over the last century and retreated more than 12 km [*Molnia*, 2008]. It is notorious for its surges, i.e., phases of accelerated flow that transports a large quantity of ice from upstream to lower elevation, typically every 25 years. The last surges took place in 1993–1995 [*Fatland and Lingle*, 1998] and 2008–2011 [*Burgess et al.*, 2012]. To the East, Seward Glacier connects with the Malaspina Glacier, the largest piedmont glacier in the world, roughly 50 km in diameter, with an intricate pattern of folded moraines. The Bering and Malaspina systems are major contributors to the total ice loss from Alaska [*Arendt et al.*, 2002]. Few ice thickness measurements have been collected on them [*Molnia*, 2008], none on Bagley or Seward.

[13] Farther east is the Hubbard Glacier, with an area of 2450 km^2, the largest nonpolar tidewater glacier in the world, more than 120 km from its origin, on the flanks of Mount Logan, Yukon, Canada to sea level where it terminates in Disenchantment Bay and Russell Fiord near Yakutat, Alaska. The terminus of Hubbard Glacier closely approaches the opposite side of Russell Fiord. In 1986 and 2002, the gap closed, creating a glacier-dammed lake, which ended with large outbursts when the ice dam failed. The glacier is grounded below sea level near its terminus [*Molnia*, 2008]. Its high accumulation to ablation area ratio (0.9), is a consequence of this glacier experiencing the advancing phase of the tidewater glacier cycle. By 1500 AD, it had retreated from its previous Little Ice Age maximum near the town of Yakutat to deep within Disenchantment Bay, near Valerie Glacier [*Barclay et al.*, 2001]. Since that retreat ended in the late 19th century, the terminus has steadily advanced.

[14] West of Bering and 30 km west of Valdez is the Columbia Glacier, one of the most studied tidewater glaciers in the U.S. Columbia started a major, possibly irreversible retreat in 1982 [*Meier and Post*, 1987]. The glacier flows from an elevation of 3050 m along the flanks of the Chugach Mountains into Prince William Sound where it terminates at a grounded calving front. The glacier has retreated 18 km since 1982, concurrent with rapid thinning. Radio echo sounding, along with depth estimates from mass conservation calculations, indicates that the bed rises above sea level 32 km upstream from the preretreat terminus [*McNabb et al.*, 2012] suggesting that the glacier may retreat another

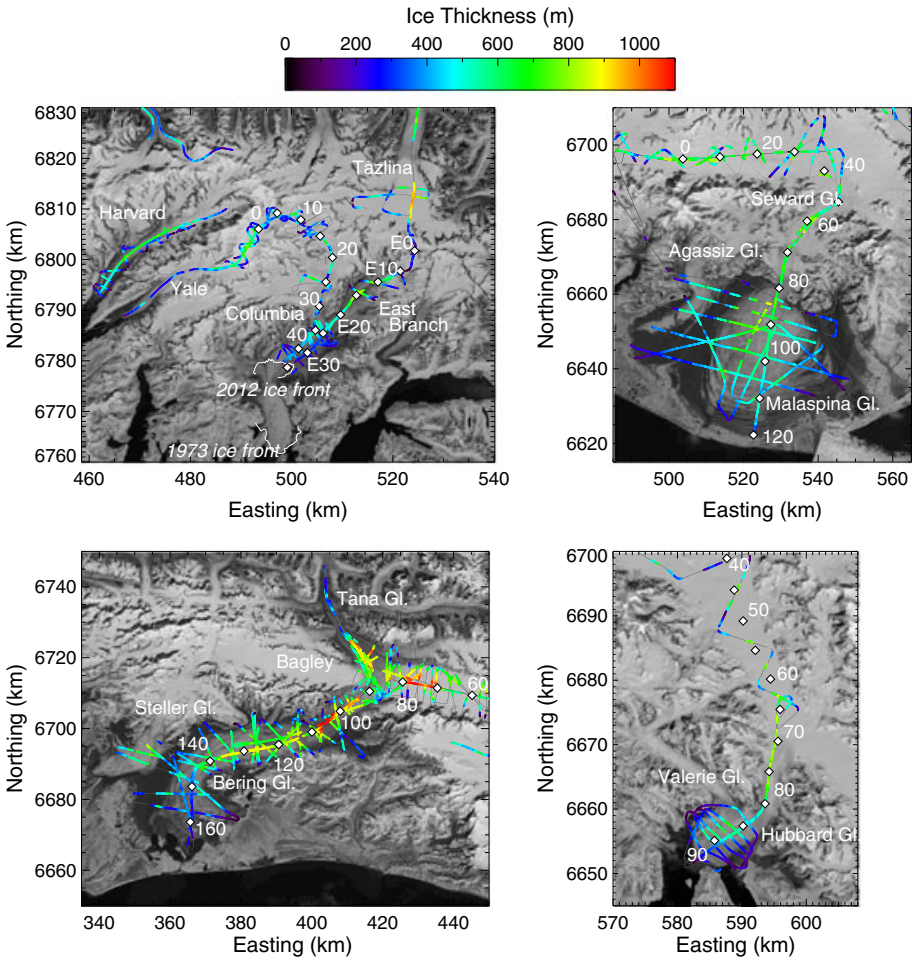

Figure 2. (continued)

15 km before it becomes disconnected from the ocean waters. The Tazlina Glacier is a large, land-terminating glacier to the north, with unknown ice thickness, ending one mile south of Tazlina Lake.

3. Results

[15] Figure 1 shows a radar echogram down the centerline of Bering Glacier. The radar echoes are affected by ringing because of the incomplete insolation of the receive and transmit antenna, which share the same wire. The surface return is absent because of the radar low flying altitude but solid bed returns are obtained over the entire length of the glacier, from 800 m thick at point A, to peak values around 1000 m in the middle, down to 200 m at point B. Around km 40, radar clutter increases significantly, which we attribute to surface scattering while passing over a section of rough, broken up, crevassed ice surface. Despite the long wavelength of WISE, 120 m in air and 67 m in ice, the glacier surface is still rough at that spatial scale.

[16] On Columbia Glacier, the main glacier branch rises above sea level at km 32, with a glacier thickness of 450 m; maximum thickness is 600 m at km 20 (icefall reach) (Figure 2). Data from the east branch however reveals a deeper bed, which is grounded below sea level until km 11, or 23 km from the 2012 ice front and 11 km farther inland than for the main branch (Figure 3). The east branch is 800 m thick when it rises above sea level and 900 m thick at km 15–17. The flight path did not follow the centerline around km 20, so the data may not have captured the thickest ice at that location. The survey also covers Harvard and Yale glaciers to the west, and Tazlina Glacier to the north. Harvard, similar to Hubbard, is in the advancing stage of the tidewater glacier cycle. Harvard is considerably thicker than Yale and grounded below sea level for 15 km. Tazlina displays some of the thickest ice in Alaska, about 1030 m in the accumulation area. (Figure 2).

[17] Data from the Bering reveals a bed that is below sea level for 52 km, until km 100 at the junction with BIV where ice is 1000 m thick, in agreement with *Conway et al.* [2009]. In our observations, ice thickness in the center section of BIV reaches 1200 m near km 70–80 and is 600–800 m deep over the next 60 km (Figure 3). Three deep, broad basins exist at km 135–125 (about 900 m thickness), 100–110 (1200 m thickness), and 70–80 (Figure 2). These basins are 5–10 km in diameter and several hundred meters deeper than the surrounding ice.

[18] For the Malaspina and Seward glaciers, the bed remains below sea level from km 120 until km 80 with a thickness of 600 m (Figures 2 and 3). Ice thickness increases to 800 m in Seward trough and 600–800 m in the accumulation area beyond km 40 with a bed elevation 1500 m above sea level. The data reveal the presence of thinner ice along the topographic divide between Agassiz and Malaspina. Our

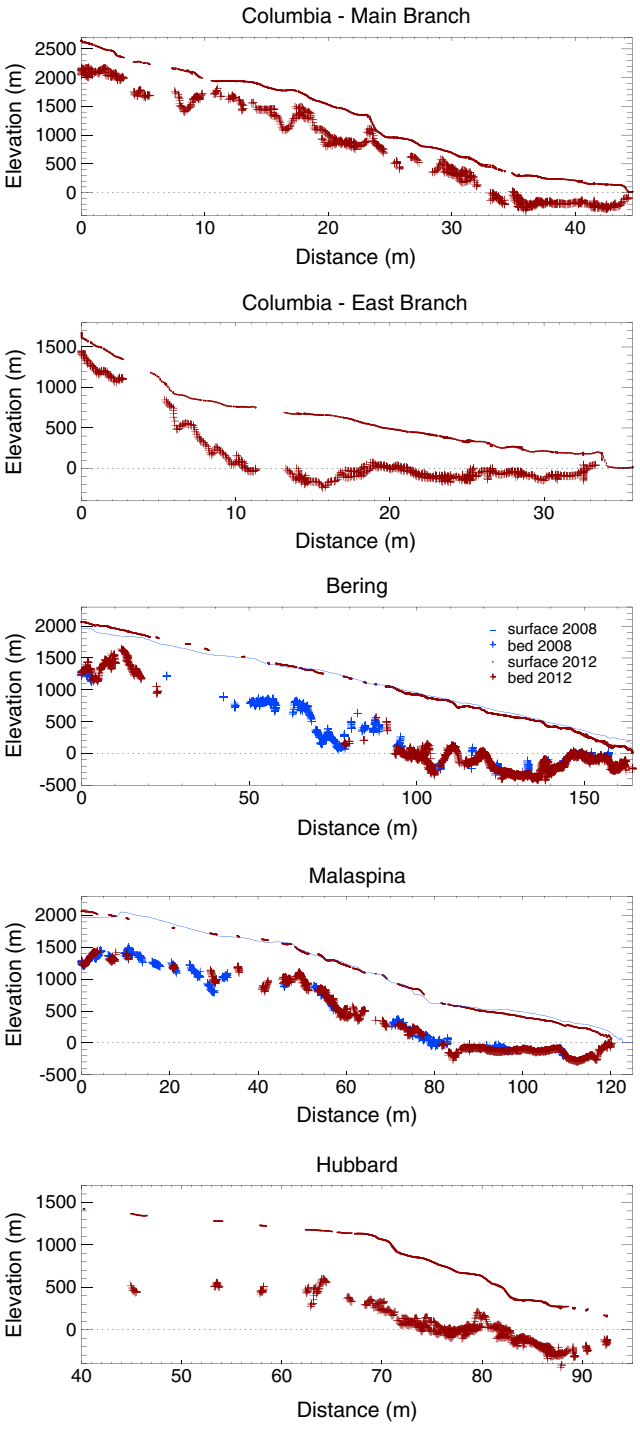

Figure 3. Bed position inferred from WISE data acquired in March 2012 (red cross) and November 2008 (blue cross), surface elevation from UAF LIDAR in March 2012 (red line) and from a reference digital elevation models in 2000 (blue line) along the approximate center line of the main branch of Columbia Glacier; the east branch of Columbia Glacier; the Bering Glacier; the Malaspina Glacier; and the Hubbard Glacier with profile location and reference distances shown in Figure 2.

profile does not follow the centerline of Seward at the junction with Malaspina (km 80), so central ice may be deeper if the valley is symmetric. The smooth bed topography of Malaspina is one of the most highly radar reflective of the entire data set, hence, indicates the presence of a wet bed since the bed is very smooth at these radar wavelengths. It forms a nearly circular depression centered in the middle of the lobe, i.e., shallower northward toward the mountains and southward toward the ice margin. The bed is as low as 350 m below sea level 10 km from the margin (km 110).

[19] Finally, the Hubbard Glacier has a terminus lobe that is grounded entirely below sea level, in agreement with prior studies [*Molnia*, 2008]. A deeper channel is present to the northwest side of the glacier, along the junction with Valerie Glacier. Surges of the Valerie tend to drive the more rapid seasonal advances of the Hubbard Terminus, including during modern closures of the Russell Fiord in 1986 and 2002 [*Ritchie et al.*, 2008]. The bed of Hubbard Glacier rises above sea level at about km 82 (Figure 3), where the glacier passes through a constriction in the St. Elias Range. But it is possible that the bed remains near sea level to km 75 given that our flight line did not always follow the glacier center; this will require confirmation using cross-glacier profiles. Ice thickness is 500 m at km 83, 800 m in the terminal valley, and reaches a local maximum of 900 m at km 70. Ice thickness remains high for the remainder of the upper part, with a maximum 950 m thickness at km 45 at 1400 m elevation. This is at about the same elevation where ice thickness is maximum on Bering Glacier.

4. Discussion

[20] For Columbia, the data suggests that the glacier may continue to retreat for several decades along the main branch but even longer along the east branch, unless the retreat is slowed by a constriction or narrow point in the fjord, which can only be addressed with more data. If the retreat continues, the glacier will be partially replaced by a 50 km long, 200–300 m deep glacial fjord. Our results are consistent with the reconstruction of ice thickness from *McNabb et al.* [2012], but we find the east branch grounded below sea level a few kilometers farther upstream.

[21] Glacier surges are short periods of fast ice motion (10–100 times normal) that occur periodically due to a buildup of driving stress during times of slower flow. Increases in driving stress alter the subglacial drainage system, which eventually reduces basal friction from increased water pressure and allows accelerated flow. Surge initiation on Bering Glacier requires regions of low driving stress and high basal drag that allow the buildup of driving stress through time. Deeper pockets of ice followed by shallow sills provide such a region [*Burgess et al.*, 2012]. In our mapping, we identify three such deeper bed portions. By comparing their location with the results of *Burgess et al.* [2012], we conclude that these three depressions and sills coincide exactly with three dynamic balance lines identified by these authors from time series of velocity and altimetry measurements without thickness data. Our mapping of bed topography therefore supports their interpretation of the surge cycle of Bering Glacier. The deeper bed portions may also be part of a complex fiord system with several channels where the

bed is below sea level intersped with areas above sea level [*Molnia*, 2008].

[22] Meltwater generated at the surface of BIV may percolate to the bed through cracks, conduits, crevasses, and moulins [*Fountain and Walder*, 1998]. The subglacial water from BIV may however experience episodically less efficient or possibly seasonally blocked drainage from the BIV because of the presence of a sill at the junction with Bering Glacier. Locally increased basal sliding across this shallowing may disrupt basal hydrology. We suggest that this configuration is one of the factors contributing to the surge nature of Bering Glacier. Once subglacial water ponding reaches a threshold above the sill, abrupt lake drainage may occur, which would trigger rapid ice motion. In that exact same region, *Fatland and Lingle* [1998] detected bull's eyes of interferometric displacement characteristic of abrupt subglacial lake drainage during the 1993–1995 surge in BIV.

[23] On the Seward Glacier, our measured ice thickness of 800 m near the approximate center line is slightly higher than the averaged ice thickness calculated by *Headley et al.* [2012], but in the absence of cross-valley profiles, our bed evaluation is incomplete. In contrast with the case of Bering Glacier, we do not detect a major bed constriction at the outset of Seward terminal valley or at the junction with the Malaspina Glacier. We do not find major bed depressions similar to those detected beneath the Bering Glacier, which may explain why the Seward is not as prone to surges as the Bering.

[24] On the Hubbard Glacier, our results are consistent with the earlier mapping of ice thickness on the glacier frontal lobe using seismic methods and ground traverse with radar sounders [*Molnia*, 2008], including the east-west bed asymmetry. To the best of our knowledge, however, our measurements are the first ice thickness measurements along the terminal valley of Hubbard Glacier and its accumulation area. Prior knowledge of glacier ice in this region placed its maximum thickness by default around 700–800 m, or the inherent limitation of ground radar systems.

[25] The data presented herein, collected over a period of 10 days, cover more ground with better precision that all prior ice thickness data ever collected in southern Alaska. Despite the lower vertical precision of our data compared to higher frequency radars, and the technical difficulties of approving the deployment of the tailing antenna component of our system, our results demonstrate its capability to obtain critical thickness data over temperate ice.

5. Conclusions

[26] We present comprehensive and complete measurements of ice thickness in southern Alaska, obtained using a low-frequency airborne radar, uniformly across the ablation and accumulation areas, for the first time. The campaigns targeted the region's largest glaciers and icefields, and the data reveal the full extent of large areas of several glaciers grounded below sea level. Variations in bed topography of critical importance to ice dynamics (e.g., on Bering Glacier) are also revealed. Overall, the deepest ice in these glaciers and icefields is considerably thicker (1000 to 1200 m) than hinted from limited ground surveys with peak penetration at around 800 m. The application of low-frequency airborne radar sounding to additional glaciers in Alaska and other temperate regions promises to be transformative of our knowledge of ice thickness and bed topography of mountain glaciers. The radar data collected during the November 2008 and March 2012 missions will be posted at the National Snow and Ice Data Center as part of NASA's Operation IceBridge.

[27] **Acknowledgments.** The 2012 deployment was funded by NASA's Operation IceBridge grant NNX11AC24G S03. The work was performed at UCI, UI, UAF, and JPL under contracts with NASA's Cryospheric Science, Planetary Instrument Definition and Development (PIDDP) and Suborbital Programs. We dedicate this study to the memory of Dr. Ali Safaeinili, the creator of WISE, who passed away in 2009.

[28] The Editor thanks Jeffrey Kargel and Bruce Molnia for their assistance in evaluating this paper.

References

Arcone, S. A., and N. E. Yankielun (2000), 1.4 GHz radar penetration and evidence of drainage structures in temperate ice: Black Rapids Glacier, Alaska, U.S.A., *J. Glaciol.*, *46*(154), 477–490.

Arendt, A. A., K. A. Echelmeyer, W. D. Harrison, C. S. Lingle, and V. B. Valentine (2002), Rapid wastage of Alaska glaciers and their contribution to rising sea level, *Science*, *297*, 382–386.

Barclay, D. J., P. E. Calkin, and G. C. Wiles (2001), Holocene history of Hubbard Glacier in Yakutat Bay and Russell Fiord, southern Alaska, *Geol. Soc. Am. Bull.*, *113*, 388–402.

Blindow, N., S. K. Suckro, M. Rückamp, M. Braun, M. Schindler, B. Breuer, H. Saurer, J. C. Simões, and M. A. Lange (2010), Geometry and thermal regime of the King George Island ice cap, Antarctica, from GPR and GPS, *Ann. Glaciol.*, *51*(55), 103–109.

Brown, C. S., L. A. Rasmussen, and M. Meier (1986), Bed topography inferred from airborne radio-echo sounding of Columbia Glacier, Alaska, *U.S. Geol. Surv. Prof. Pap. 1258-G*, 32 pp.

Burgess, E. W., R. R. Forster, C. F. Larsen, and M. Braun (2012), Surge dynamics on Bering Glacier, Alaska, in 2008–2011, *The Cryosphere*, *6*, 1251–1262.

Clarke, T., and K. Echelmeyer (1996), Seismic-reflection evidence for a deep subglacial trough beneath Jakobshavns Isbrre, West Greenland, *J. Glaciol.*, *43*(141), 219–232.

Conway, H., B. Smith, P. Vaswani, K. Matsuoka, E. Rignot, and P. Claus (2009), A low-frequency ice-penetrating radar system adapted for use from an airplane: Test results from Bering and Malaspina Glaciers, Alaska, USA, *Ann. Glaciol.*, *50*(51), 93–97.

Fatland, D. R., and C. S. Lingle (1998), Analysis of the 1993–95 Bering Glacier (Alaska) surge using differential SAR interferotnetry, *J. Glaciol.*, *44*(148), 532–546.

Fountain, A. G., and J. S. Walder (1998), Water flow through temperate glaciers, *Rev. Geophys.*, *36*(3), 299–328.

Gades, A. M., C. F. Raymond, and H. Conway (2012), Radio-echo probing of Black Rapids Glacier, Alaska, USA, during onset of melting and spring speed-up, *J. Glaciol.*, *58*(210), 713–724.

Gogineni, S., D. Tammana, D. Braaten, C. Leuschen, T. Akins, J. Legarsky, P. Kanagaratnam, J. Stiles, C. Allen, and K. Jezek (2001), Coherent radar ice thickness measurements over the Greenland ice sheet, *J. Geophys. Res.*, *106*(D24), 33,761–33,772, doi:10.1029/2001JD900183.

Headley, E., B. Hallet, G. Roe, E. D. Washington, and E. Rignot (2012), Spatial distribution of glacial erosion rates in the St. Elias range, Alaska, inferred from a realistic model of glacier dynamics, *J. Geophys. Res.*, *117*, F03027, doi:10.1029/2011JF002291.

Jacob, T., J. Wahr, W. T. Pfeffer, and S. Swenson (2012), Recent contributions of glaciers and ice caps to sea level rise, *Nature*, *482*, 514–518.

Johnson, A. J., C. F. Larsen, N. Murphy, A. Arendt, and S. L. Zirnheld (2013), Mass balance in the Glacier Bay area of Alaska, USA, and British Columbia, Canada, 1995–2011, using airborne laser altimetry, *J. Glaciol.*, *59*(216), 632–648.

Jordan, R., et al. (2009), The Mars express MARSIS sounder instrument, *Planet. Space Sci.*, *57*, 1975–1986.

McNabb, R. W., et al. (2012), Using surface velocities to calculate ice thickness and bed topography: A case study at Columbia Glacier, Alaska, USA, *J. Glaciol.*, *58*(212), 1151–1164.

Meier, M. F., and A. Post (1987), Fast tidewater glaciers, *J. Geophys. Res.*, *92*(B9), 9051–9058.

Molnia, B. F. (2008), Glaciers of North America: Glaciers of Alaska, in *Satellite Image Atlas of Glaciers of the World, (USGS Professional Paper*

1386-K), edited by R. S. Williams Jr. and J. G. Ferrigno, 521 pp., U.S. Geol. Surv., Washington, D. C.

Muskett, R. R., C. S. Lingle, J. M. Sauber, A. S. Post, W. V. Tangborn, B. T. Rabus, and K. A. Echelmeyer (2009), Airborne and spaceborne DEM- and laser altimetry-derived surface elevation and volume changes of the Bering Glacier system, Alaska, USA, and Yukon, Canada, 1972–2006, *J. Glaciol.*, *55*(190), 316–326.

Ritchie, J. B., C. S. Lingle, R. J. Motyka, and M. Truffer (2008), Seasonal fluctuations in the advance of a tidewater glacier and potential causes: Hubbard Glacier, Alaska, USA, *J. Glaciol.*, *54*(186), 401–411.

Smith, B. M. E., and S. Evans (1972), Radio echo sounding: Absorption and scattering by water inclusions and ice lenses, *J. Glaciol.*, *11*(61), 133–146.

Stolt, R. H. (1978), Migration by Fourier transform, *Geophysics*, *43*, 23–48.

Watts, R. D., and A. W. England (1976), Radio-echo sounding of temperate glaciers: Ice properties and sounder design criteria, *J. Glaciol.*, *17*(75), 39–48.